

# Towards Robust Airborne SLAM in Unknown Wind Environments

**Jonghyuk Kim**

Department of Engineering  
Australian National University, Australia  
jonghyuk.kim@anu.edu.au

**Salah Sukkarieh**

ARC Centre for Autonomous Systems  
University of Sydney, Australia  
salah@acfr.usyd.edu.au

## Abstract

This paper presents a robust multi-loop airborne SLAM structure which augments wind information into the state of 6DoF Simultaneous Localisation and Mapping (SLAM). The relative air velocity observation from an air data system can be used to estimate the error of the vehicle state. However due to *a priori* unknown wind information, it cannot directly be used for that purpose. This can be tackled by augmenting this information into SLAM and estimating it simultaneously with the vehicle state. This can significantly increase the consistency of airborne SLAM at the time of loop closure. The air velocity based SLAM loop limits the error growth of the velocity and attitude effectively and the feature based SLAM loop bounds the position error growth. Simulation results show that wind information can be estimated consistently and the robustness of airborne SLAM improves significantly.

## 1 Introduction

SLAM has been demonstrated and verified in many robotic applications as in indoor, land and underwater environments [Williams and Mahon, 2004][Nuchter *et al.*, 2004][Chatila *et al.*, 2004]. Airborne SLAM is to expand this concept to the 6DoF (Degrees of Freedom) aerial vehicles. It incrementally builds an environmental map and simultaneously utilising this map to estimate the vehicle state. Due to the 6DoF nature that the vehicle undergoes, the conventional dead reckoning sensors cannot be applied here. Instead Inertial Measurement Unit (IMU) and Inertial Navigation System (INS) should be incorporated as shown in [Kim, 2004]. In addition, the computationally intensive INS loop makes it intractable to implement SLAM in its direct form. This has been tackled by exploiting the low-dynamic nature of INS errors resulting in an indirect SLAM [Kim and Sukkarieh, 2004b].

The current obstacle in implementing a robust airborne SLAM is the inconsistency problem related with the closing-the-loop after long flight. The limited field of view of the airborne sensor and the sparse nature of the feature observations can inevitably increase the vehicle's uncertainties before the loop closure. The position error growth rate of the unaided INS is typically cubic function of the flight time. This means there can be large uncertainties in the vehicle states when it tries to close the loop. However the large uncertainties can easily destroy the linearisation assumption in the SLAM filter, and any over-confident attitude correction can lead to a failure in SLAM. This is due to the fact that even a small attitude error will misinterpret the gravitational acceleration, thus resulting in a rapid divergence in the position and velocity. This, in turn, will easily invalidate and reject successive observations afterward.

This problem can be tackled by using a more high-quality IMU, non-linear filtering, or adding additional information to stabilise the attitude. If a high-quality IMU is an available option it should be selected in such a way that the INS error remains within a reasonable bound before closing the loop. The INS error growth, however, depends on the availability of the features which is difficult to predict in advance. Additionally, many high-quality inertial sensors may not be a suitable option for most robotic platforms which are payload limited. The nonlinear filter, such as particle filter, can reduce the chance of divergence during the closing the loop. It was observed that it can improve the performance compared to the standard Kalman filter, but it still showed inconsistency during the closing the loop. It also suffers the dimensionality problem. The effectiveness of this approach needs further investigations in airborne SLAM applications.

The stability of the attitude estimate is of importance for the reliable closing the loop. Hence if there exists any constant stream of information to limit the attitude uncertainty, it can improve the robustness of airborne SLAM. In many airborne applications, the air veloc-

ity observation is directly available from the onboard air-data system, which comprises a pitot tube and alpha/beta vanes with data acquisition system. It provides airspeed, angle of attack and side-slip angle which are important to maintain the aircraft stability. The air velocity vector, which is a relative velocity with respect to the wind vector, can be computed from these observations. The wind velocity, however, is typically a priori unknown quantity. Hence it cannot directly be used to aid INS. One solution, proposed in this paper, is to augment this unknown wind velocity into the SLAM state vector and to estimate it simultaneously, utilising it to estimate INS error. Although this method adds extra information to the system, it does not require further physical hardware but an modification in algorithm. Another benefit is that the air-data system is a self-contained system and the autonomy of SLAM can still be maintained.

Figure 1 describes the multiple loop SLAM architecture with the indirect framework. The high frequent ( $\geq 100\text{Hz}$ ) INS loop provides real-time vehicle states to external guidance and control logics. The medium frequent air-data observation ( $\geq 10\text{Hz}$ ) estimates wind velocity and stabilises the velocity/attitude forming an velocity based SLAM loop. The attitude error is estimable from the correlation structure between the velocity and attitude errors. It, however, does not provide any information to the position error. Hence the aperiodic feature observation is required to estimate the SLAM position error. The indirect formulation makes it a simple task to augment any other aiding information such as GNSS [Kim and Sukkarieh, 2004a].

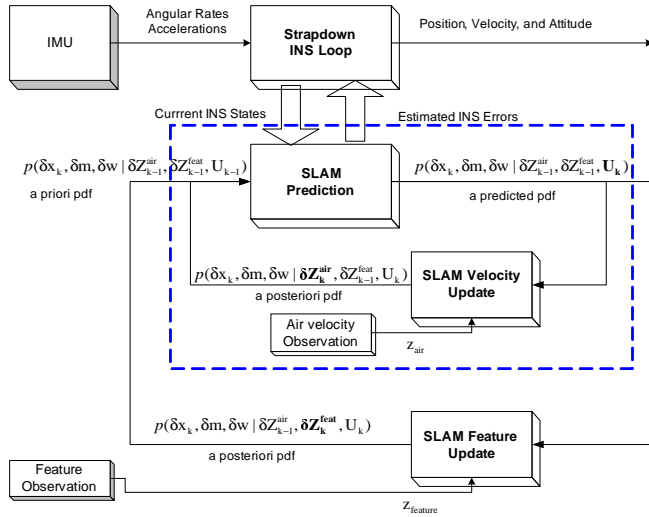


Figure 1: Multi-loop architecture of airborne SLAM: the inner-periodic SLAM loop (within a broken box) is for velocity/attitude stabilisation and the outer-aperiodic SLAM loop is for feature observation update.

This paper is organised as follows: Section 2 will briefly present the high speed inertial navigation loop. Section 3 will provide a Bayesian formulation of the indirect airborne SLAM with unknown wind velocity augmentation. Section 4 will describe the Kalman Filter (KF) implementation with the details of the air-data observation. Sections 5 and 6 will provide the results of simulation analysis for the Brumby MkIII UAV platform, then Section 7 will conclude with future works.

## 2 Inertial Navigation Loop

In the indirect airborne SLAM architecture, The INS loop predicts the high-dynamic vehicle states from IMU measurements in real-time. The SLAM filter resides outside the loop and performs an aiding role. The quaternion-based strapdown INS algorithm is used with an assumption of flat and non-rotating frame. This is a reasonable assumption for the low quality inertial, low speed, and short coverage (typically within  $100\text{Km}$ ) applications. The discrete equation can be written as

$$\begin{bmatrix} \mathbf{p}^n(k+1) \\ \mathbf{v}^n(k+1) \\ \mathbf{q}^n(k+1) \end{bmatrix} = \begin{bmatrix} \mathbf{p}^n(k) + \mathbf{v}^n(k)\Delta t \\ \mathbf{v}^n(k) + [(\mathbf{C}_b^n(\mathbf{q}^n(k))\bar{\mathbf{f}}^b(k) + \mathbf{g}^n)]\Delta t \\ \mathbf{q}^n(k) \otimes \Delta\mathbf{q}^n(k) \end{bmatrix}$$

with  $\mathbf{p}^n(k)$ ,  $\mathbf{v}^n(k)$ ,  $\mathbf{q}^n(k)$  representing position, velocity, and quaternion respectively at discrete time  $k$ ,  $\Delta t$  being the time for update interval,  $\mathbf{q}^n(k)$  being the attitude quaternion with  $\otimes$  for the quaternion multiplication, and  $\Delta\mathbf{q}^n(k)$  being a delta quaternion computed from gyroscope readings during the attitude update interval.

The wind velocity and feature map are maintained outside the SLAM filter and are treated as external databases.

## 3 Bayesian Model for Indirect SLAM

The airborne SLAM problem with unknown wind velocity and map needs to compute the probability density function, given all observations and control inputs up to current time  $k$ . In indirect SLAM, only the probability function for the error variables are of interest:

$$p(\delta\mathbf{x}_k, \delta\mathbf{m}, \delta\mathbf{w} | \delta\mathbf{Z}_k, \mathbf{U}_k) \quad (1)$$

where,

$\delta\mathbf{x}_k$  is a vehicle state such as position, velocity and attitude

$\delta\mathbf{m}$  is a stationary map position

$\delta\mathbf{w}$  is a wind velocity vector

$\delta\mathbf{Z}_k$  is a feature and air velocity observation:

$$\delta\mathbf{Z}_k = \{\delta\mathbf{Z}_k^f, \delta\mathbf{Z}_k^a\} = \{z_0^f, z_1^f, \dots, z_k^f, z_0^a, z_1^a, \dots, z_a^f\}$$

$\mathbf{U}_k$  is an inertial sensor observation:

$$\mathbf{U}_k = \{u_0, u_1, \dots, u_k\}$$

From the Bayes theorem, the *a posteriori* distribution can be obtained from the likelihood and predicted distribution,

$$\begin{aligned}
& p(\delta \mathbf{x}_k, \delta \mathbf{m}, \delta \mathbf{w} \mid \delta \mathbf{Z}_k, \mathbf{U}_k) \\
& \propto p(\delta \mathbf{z}_k^f, \delta \mathbf{z}_k^a \mid \delta \mathbf{x}_k, \delta \mathbf{m}, \delta \mathbf{w}) p(\delta \mathbf{x}_k, \delta \mathbf{m}, \delta \mathbf{w} \mid \delta \mathbf{Z}_{k-1}, \mathbf{U}_k) \\
& = p(\delta \mathbf{z}_k^f \mid \delta \mathbf{x}_k, \delta \mathbf{m}, \delta \mathbf{w}) p(\delta \mathbf{z}_k^a \mid \delta \mathbf{x}_k, \delta \mathbf{m}, \delta \mathbf{w}) \\
& \quad \times p(\delta \mathbf{x}_k, \delta \mathbf{m}, \delta \mathbf{w} \mid \delta \mathbf{Z}_{k-1}, \mathbf{U}_k) \\
& = p(\delta \mathbf{z}_k^f \mid \delta \mathbf{x}_k, \delta \mathbf{m}) \times \underbrace{p(\delta \mathbf{z}_k^a \mid \delta \mathbf{x}_k, \delta \mathbf{w}, \delta \mathbf{Z}_{k-1}, \mathbf{U}_k)}_{\text{high velocity-obs update}} \\
& \quad \underbrace{\hspace{10em}}_{\text{low feature obs-update}}
\end{aligned}$$

where the property of conditional independence between the feature and air velocity observation is used and it is assumed that the feature observation is synchronised to velocity observation.

From these factored update form, the periodic velocity based inner SLAM loop can be separated from the aperiodic feature based outer SLAM loop as shown in Figure 1.

## 4 Indirect SLAM Implementation

In this paper, Kalman filter is used to implement the indirect airborne SLAM by using the linearised SLAM error model [Kim and Sukkarieh, 2004b].

The linearised SLAM system in discrete time can be written as

$$\begin{aligned}
\delta \mathbf{x}(k+1) &= \mathbf{F}(k) \delta \mathbf{x}(k) + \mathbf{G}(k) \mathbf{w}(k) \quad (2) \\
\delta \mathbf{z}(k) &= \mathbf{H}(k) \delta \mathbf{x}(k) + \mathbf{v}(k), \quad (3)
\end{aligned}$$

where  $\delta \mathbf{x}$  is the error state vector,  $\mathbf{F}(k)$  is the time-varying state transition matrix,  $\mathbf{G}(k)$  is the system noise input matrix and  $\mathbf{w}(k)$  is the system noise vector which represents any un-modelled instrument errors with noise strength  $\mathbf{Q}(k)$ .  $\mathbf{H}(k)$  is the linearised observation Jacobian and  $\mathbf{v}(k)$  is the observation noise with noise strength matrix  $\mathbf{R}(k)$ . The error observations are generated by subtracting the measured quantity  $\tilde{\mathbf{z}}(k)$  from the INS predicted quantity  $\hat{\mathbf{z}}(k)$ ,

$$\delta \mathbf{z}(k) = \hat{\mathbf{z}}(k) - \tilde{\mathbf{z}}(k). \quad (4)$$

The state consists of the errors in INS, wind velocity, and map:

$$\delta \mathbf{x}(k) = [\delta \mathbf{x}_{ins}(k) \quad \delta \mathbf{v}_{wind}(k) \quad \delta \mathbf{x}_{map}(k)]^T. \quad (5)$$

The error state of INS,  $\delta \mathbf{x}_{ins}(k)$ , comprises the errors in the INS indicated position, velocity and attitude expressed in the navigation frame which is defined with north, east and down axes at the current vehicle position:

$$\delta \mathbf{x}_{ins}(k) = [\delta \mathbf{p}^n(k) \quad \delta \mathbf{v}^n(k) \quad \delta \boldsymbol{\psi}^n(k)]^T. \quad (6)$$

The error state vector of the wind velocity is also defined in the navigation frame. A constant velocity model is used in this paper and a more precise model can be incorporated [Stevens and Lewis, 1992]. The error state of map,  $\delta \mathbf{x}_{map}(k)$ , comprises the errors in 3D feature positions in the navigation frame. A stationary model is used and the size of the state is dynamically augmented with the new feature.

The resulting detailed discrete state transition matrix  $\mathbf{F}(k)$  and the noise transfer function  $\mathbf{G}(k)$  can be found in [Kim, 2004].

### 4.1 Feature Observation

The on-board feature observation sensor provides range ( $\rho$ ), bearing ( $\varphi$ ), and elevation ( $\vartheta$ ) between the vehicle and feature. The nonlinear observation equation relates these observations to the state through the Cartesian to polar transformation, and the navigation to sensor frame transformation [Kim, 2004]. The sensor frame is assumed to be aligned to the body frame. The observation can then be predicted from the relative position vector between the feature and vehicle:

$$\hat{\mathbf{z}}_{feature}^s(k) = [\hat{\rho} \quad \hat{\varphi} \quad \hat{\vartheta}]^T \quad (7)$$

$$= \begin{bmatrix} \sqrt{\hat{x}^2 + \hat{y}^2 + \hat{z}^2} \\ \arctan(\hat{y}/\hat{x}) \\ \arcsin(\hat{z}/\hat{\rho}) \end{bmatrix} \quad (8)$$

where the relative position vector is

$$[\hat{x} \quad \hat{y} \quad \hat{z}]^T = \mathbf{C}_n^b [\hat{\mathbf{m}}^n - \hat{\mathbf{p}}^n] \quad (9)$$

The linearised  $\mathbf{H}(k)$  with respect to the current vehicle and map state can be derived from the Jacobian of these nonlinear observation equations,

$$\mathbf{H}(k) = \begin{bmatrix} \frac{\partial \rho}{\partial \mathbf{p}^n} & \frac{\partial \rho}{\partial \mathbf{v}^n} & \frac{\partial \rho}{\partial \boldsymbol{\psi}^n} & \left| \begin{array}{c} 0_{1 \times 3} \\ 0_{1 \times 3} \\ 0_{1 \times 3} \end{array} \right. & \left| \begin{array}{ccc} \cdots & -\frac{\partial \rho}{\partial \mathbf{p}^n} & \cdots \\ \cdots & -\frac{\partial \rho}{\partial \mathbf{v}^n} & \cdots \\ \cdots & -\frac{\partial \rho}{\partial \boldsymbol{\psi}^n} & \cdots \end{array} \right. \end{bmatrix} \quad (10)$$

with corresponding sensor noise variance

$$\mathbf{R}(k) = \begin{bmatrix} \sigma_\rho^2 & 0 & 0 \\ 0 & \sigma_\varphi^2 & 0 \\ 0 & 0 & \sigma_\vartheta^2 \end{bmatrix}. \quad (11)$$

### 4.2 Air-Data Observation

The on-board air-data system can deliver air speed ( $V$ ), angle of attack ( $\alpha$ ), and side slip angle ( $\beta$ ) from the pitot tube and alpha/beta vanes [Stevens and Lewis, 1992]. Figure 2 describes the typical pitot system and the geometry of the aerodynamic angles. The pitot tube is typically installed on the front nose or wing tip in push-prop type vehicles.

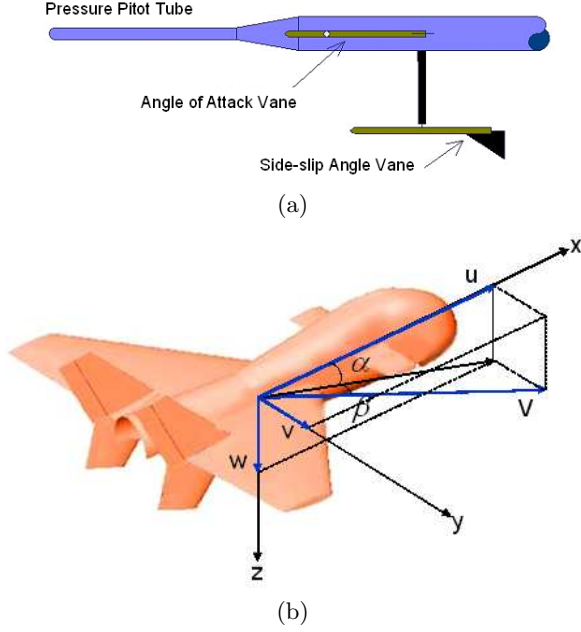


Figure 2: a) A pitot tube for pressure measurement with alpha/beta vanes for aerodynamic angles. b) The geometry of the air velocity vector with the aerodynamic angles.

The pressure measurements can be converted into the airspeed which is the vehicle velocity with respect to the ambient air mass. By using the observation geometry, the air velocity vector in the body frame  $\mathbf{v}_{air}^b$  can be constructed,

$$\mathbf{v}_{air}^b = [u \ v \ w]^T \quad (12)$$

$$= \begin{bmatrix} V \cos(\alpha) \cos(\beta) \\ V \sin(\beta) \\ V \sin(\alpha) \cos(\beta) \end{bmatrix}. \quad (13)$$

By taking an inverse of this equation, the air velocity observation  $(\hat{V}, \hat{\alpha}, \hat{\beta})$  can be predicted from the relative air velocity in the body frame  $(\hat{u}, \hat{v}, \hat{w})$ ,

$$\hat{\mathbf{z}}_{air}^b = \begin{bmatrix} \hat{V} & \hat{\alpha} & \hat{\beta} \end{bmatrix}^T \quad (14)$$

$$= \begin{bmatrix} \sqrt{\hat{u}^2 + \hat{v}^2 + \hat{w}^2} \\ \arctan(\hat{w}/\hat{u}) \\ \arcsin(\hat{v}/\hat{V}) \end{bmatrix}, \quad (15)$$

where, the relative air velocity is predicted by subtracting the estimated wind velocity from the estimated INS velocity, and by transforming it into the body frame,

$$[\hat{u} \ \hat{v} \ \hat{w}]^T = \mathbf{C}_n^b [\hat{\mathbf{v}}_{ins}^n - \hat{\mathbf{v}}_{wind}^n]. \quad (16)$$

The linearised observation model is obtained by taking

Jacobian of these nonlinear equations,

$$\mathbf{H}(k) = \begin{bmatrix} 0_{1 \times 3} & \frac{\partial V}{\partial \mathbf{v}^n} & \frac{\partial V}{\partial \psi^n} & \left| \begin{array}{c} -\frac{\partial V}{\partial \mathbf{v}^n} \\ -\frac{\partial \alpha}{\partial \mathbf{v}^n} \\ -\frac{\partial \beta}{\partial \mathbf{v}^n} \end{array} \right| & 0_{1 \times 3m} \\ 0_{1 \times 3} & \frac{\partial \alpha}{\partial \mathbf{v}^n} & \frac{\partial \alpha}{\partial \psi^n} & \left| \begin{array}{c} -\frac{\partial \alpha}{\partial \mathbf{v}^n} \\ -\frac{\partial \beta}{\partial \mathbf{v}^n} \end{array} \right| & 0_{1 \times 3m} \\ 0_{1 \times 3} & \frac{\partial \beta}{\partial \mathbf{v}^n} & \frac{\partial \beta}{\partial \psi^n} & \left| \begin{array}{c} -\frac{\partial \beta}{\partial \mathbf{v}^n} \end{array} \right| & 0_{1 \times 3m} \end{bmatrix} \quad (17)$$

$$\mathbf{R}(k) = \begin{bmatrix} \sigma_V^2 & 0 & 0 \\ 0 & \sigma_\alpha^2 & 0 \\ 0 & 0 & \sigma_\beta^2 \end{bmatrix}. \quad (18)$$

Note the similarity between the feature and air velocity observation models due to the nature of three dimensional vector observations. Hence the previously developed code for the feature observation can be re-used for the air velocity observation with minimal modification.

### 4.3 Error Feedback Correction

The corrected position,  $\mathbf{p}^n(k|k)$ , and velocity,  $\mathbf{v}^n(k|k)$ , are computed by subtracting the estimated INS errors from the current INS outputs:

$$\mathbf{p}^n(k|k) = \mathbf{p}^n(k) - \delta \mathbf{p}^n(k|k) \quad (19)$$

$$\mathbf{v}^n(k|k) = \mathbf{v}^n(k) - \delta \mathbf{v}^n(k|k). \quad (20)$$

The corrected quaternion,  $\mathbf{q}(k|k)$ , is obtained by pre-multiplying the error quaternion to the current quaternion:

$$\mathbf{q}(k|k) = \delta \mathbf{q}(k|k) \otimes \mathbf{q}(k) \quad (21)$$

$$\delta \mathbf{q}(k|k) \approx [1 \ \delta \psi_x/2 \ \delta \psi_y/2 \ \delta \psi_z/2]^T \quad (22)$$

The wind velocity are directly corrected by subtracting the estimated wind velocity error from the current wind velocity:

$$\mathbf{v}_w^n(k|k) = \mathbf{v}_w^n(k) - \delta \mathbf{v}_w^n(k|k). \quad (23)$$

The map positions are also corrected by subtracting the estimated map position errors from the current positions:

$$\mathbf{x}_m^n(k|k) = \mathbf{x}_m^n(k) - \delta \mathbf{x}_m^n(k|k). \quad (24)$$

## 5 Simulation Description

A computer simulation is performed to verify the robustness of the proposed method for the Brumby UAV system developed in Australian Centre for Field Robotics (ACFR). The flight scenario is that the vehicle undergoes two racehorse tracks approximately 100m above the ground. The flight time is 340 seconds and the average flight speed is 40m/s. There are 40 features placed on the ground.

The wind is a prior unknown to the vehicle and has a magnitude of 5.0m/s with southern direction. Inside

the SLAM filter, this unknown wind velocity is estimated from the relative velocity observation. The air data sensors run at  $20\text{Hz}$  and the airspeed has a noise value of  $1\text{m/s}$ , the alpha vane and beta vane angles have noise values of  $2^\circ$  respectively.

A low-cost IMU is simulated with a sampling rate of  $400\text{Hz}$  and has an average noise values of  $0.5\text{m/s}^2$  for the accelerometers and  $0.5^\circ/\text{s}$  for the gyros. The vision sensor is used to measure the range, azimuth and elevation angles to each feature on the ground. The vision sensors run at 10 frames/s and have a horizontal field of view of  $40^\circ$  and a vertical field of view of  $30^\circ$ . In the simulation we assume known data association of the map features.

## 6 Simulation Results

Figure 3 compares the horizontal position results between unaided inertial, velocity based SLAM and velocity/feature-based, or multi-loop, SLAM. The velocity based SLAM can limit the error growth of the velocity and attitude but not the position error. By fusing the feature observation the multi-loop SLAM can estimate the position error.

Figure 4 compares the  $1\sigma$  covariances between the unaided inertial, velocity based SLAM, and multi-loop SLAM. The position and velocity along the north axis are plotted and the attitude along the yaw axis is shown. It can be observed that the velocity and attitude performances are improved in the velocity based SLAM loop. It however shows that the position error increases without bound. The feature observation provides additional position information to the vehicle state and improves overall performance.

Figure 5 shows the Monte-Carlo analysis results for the wind velocity and attitude estimates in the multi-loop SLAM. The Monte-Carlo method is used to see the statistical consistency of the SLAM filter particularly during the loop closure. Figure 5(a) shows ten runs results along the north axis with  $3\sigma$  bound. The true wind velocity was  $[-5, 0, 0]^T(\text{m/s})$ . It can be observed that the unknown wind vector can be estimated consistently during the first loop closure which is around 70 seconds. An interesting thing is the loop closure also improves the wind velocity estimate. This is due to the fact that INS has developed a cross-correlation between the position and velocity during the flight and any position improvement affects the velocity as well. Figures 5(b) and (c) show the Monte-Carlo results for the roll and yaw angles during the first loop closure. Angles from ten runs are plotted with  $3\sigma$  bounds respectively. These shows consistent angle estimates of the vehicle within the bounds. This is important in airborne SLAM since the attitude estimate can now be less susceptible to the availability and quality of the ground features.

These results shows that the multi-loop SLAM has a capability to estimate the unknown wind velocity reliably and more importantly the consistency of SLAM can be significantly improved when it tries to close the loop.

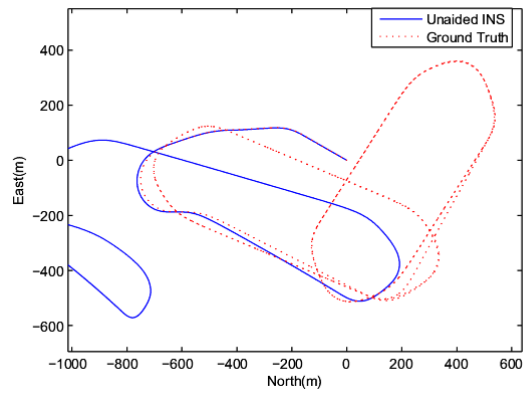
## 7 Conclusions

This paper presented a multi-loop SLAM structure to improve the consistency of the airborne SLAM. The inner SLAM loop was configured by using the periodic air-velocity update and the outer SLAM loop by the aperiodic feature update. The unknown wind velocity was augmented and estimated from the inner SLAM loop to stabilised the INS velocity and attitude. The feature observation update was still required to estimate the error growth in the INS position. The Monte-Carlo analysis verified that multi-loop SLAM is statistically consistent during the loop closure. This result can also be directly applicable to the underwater inertial SLAM problem. That is, the relative velocity measurement with respect to the underwater current can be used to stabilise SLAM. The future works can be incorporating a more precise wind model and verifying this concept for the real flight data.

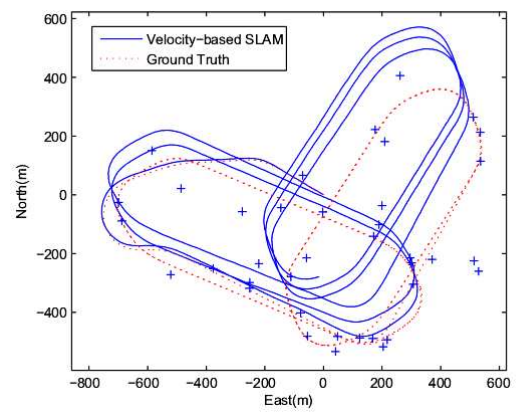
## References

- [Chatila *et al.*, 2004] R. Chatila, M.Devy, and J.D. Tardos. *SLAM 2004 Summer School: Lecture Notes*. LAAS, Toulouse, France, 2004.
- [Kim and Sukkarieh, 2004a] J. Kim and S. Sukkarieh. Complementary SLAM aided GPS/INS Navigation in GNSS Denied and Unknown Environments. In *International Symposium on GNSS/GPS*, Sydney, Australia, 2004.
- [Kim and Sukkarieh, 2004b] J. Kim and S. Sukkarieh. Improving the Real-Time Efficiency of Inertial SLAM and Understanding its Observability. In *IEEE/RSJ International Conference on Intelligent Robots and Systems*, Sendai, Japan, 2004.
- [Kim, 2004] J. Kim. *Autonomous Navigation for Airborne Applications*. PhD thesis, Australian Centre for Field Robotics, The University of Sydney, 2004.
- [Nuchter *et al.*, 2004] A. Nuchter, Surmann H., Lingenmann K., Hertzberg J., and Thurn S. 6D SLAM with an Application in Autonomous Mine Mapping. *IEEE Transactions on Robotics and Automation*, pages 1998–2003, 2004.
- [Stevens and Lewis, 1992] B.L. Stevens and F.L. Lewis. *Aircraft Control and Simulation*. John Wiley and Sons, Inc, 1992.
- [Williams and Mahon, 2004] S. Williams and I. Mahon. Simultaneous localization and mapping on the Great

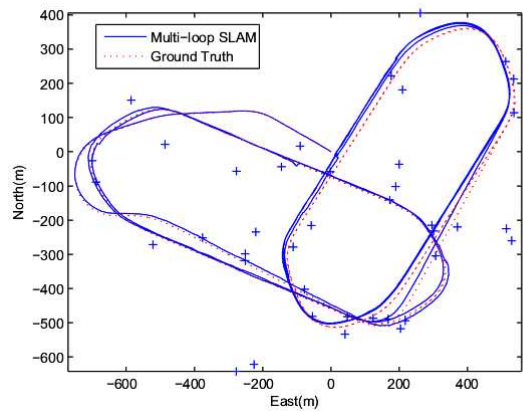
Barrier Reef. In *IEEE International Conference on Robotics and Automation*, 2004.



(a)

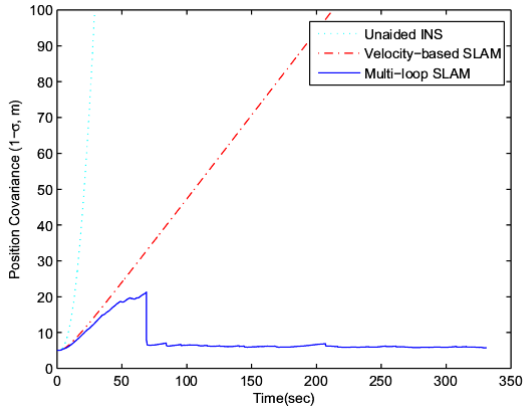


(b)

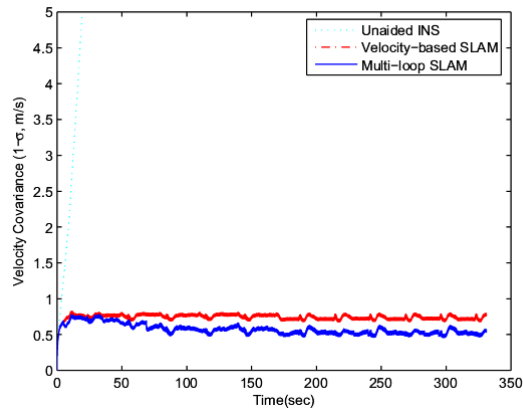


(c)

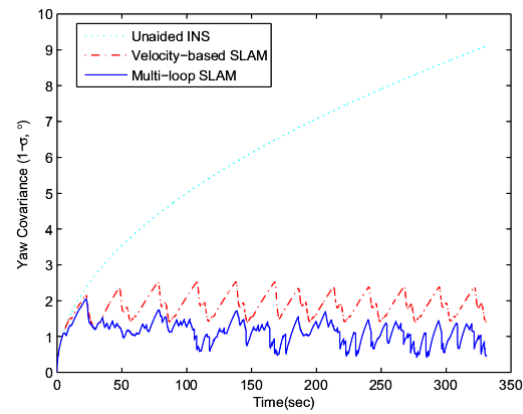
Figure 3: A comparison of 2D position results between unaided inertial, velocity based SLAM, and velocity/feature based SLAM. The velocity based SLAM improves the velocity and attitude estimates but the position still drifts. The multi-loop SLAM overcomes this and improves the filter stability.



(a)

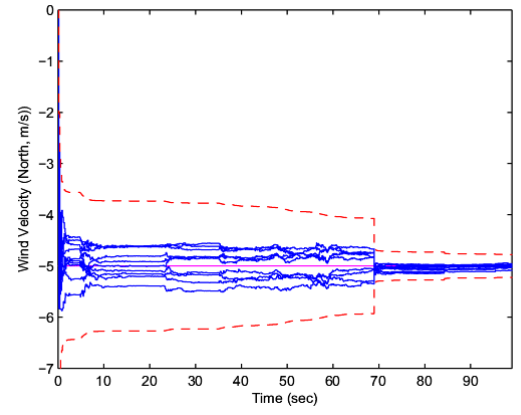


(b)

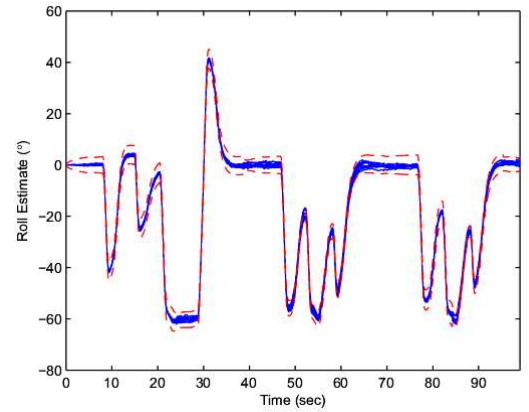


(c)

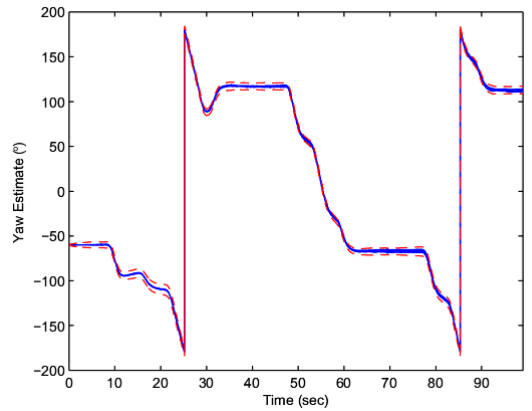
Figure 4: Comparisons of error covariances between unaided inertial, velocity based SLAM, and velocity/feature-based SLAM. The multi-loop SLAM improves the overall performances in the position, velocity and attitude.



(a)



(b)



(c)

Figure 5: a) A wind velocity estimation result in multi-loop SLAM from the Monte-Carlo analysis. The true wind velocity is  $5m/s$  southward. The estimated wind velocities from ten runs are plotted with  $3-\sigma$  uncertainty. Monte-Carlo analysis results for b) roll and c) yaw angles with  $3-\sigma$  bounds showing a consistent loop closure.